Cover Page

Universiteit Leiden

The handle http://hdl.handle.net/1887/20273 holds various files of this Leiden University dissertation.

Author: Elmalk, Abdalmohsen
Title: Exposing biomolecular properties one molecule at a time
Date: 2012-12-13

Chapter 4

Enhancement and quenching of the fluorescence of labeled single proteins immobilized on gold nanoparticles[†]

Summary. *We report on a new method to measure the redox activity of oxido-reductases as a function of time at the single molecule level under high amplicification and with increased sensitivity. The enzymes are fluorescently labeled so that the fluorescence intensity of the label reflects the redox state of the enzyme's active site. Amplification is realized by immobilization of enzyme molecules on gold nanoparticles (AuNPs). The method is illustrated by using a labeled 14 kDa large copper protein (i.e., azurin (Az) from Pseudomonas aeruginosa) and immobilizing it on gold AuNPs of varying size (1.4-80 nm). The Zn substituted variant is used as a control. Intensity and life time variations are analyzed quantitatively by taking into account the influence of the AuNP on the fluorophore excitation rate and quantum yield. Attachment of fluorescently labeled CuAz to a AuNP may lead to a tenfold enhancement of the sensitivity for detecting a redox change of the protein. These findings open new ways to study hitherto unexplored mechanistic details of oxido-reductases. They are also of relevance for the design of biosensors and devices for electronic data storage.*

1. Introduction

Nanoparticles (NPs) of noble metals like Au and Ag have been at the center of attention[1-12] (see also reviews[13-15] and references therein) because of their unique optical properties. These properties derive from the collective oscillation of the confined conduction electrons. Surface plasmon resonance (SPR) gives rise to absorption in the visible region with very high extinction coefficients (typically 10^9 M^{-1} cm^{-1} at around 500 nm for a 20 nm AuNP, for instance[16]), very intense Rayleigh scattering, and a strong enhancement of the local electric field near the nanoparticle surface[13, 17-21]. Because of these properties, the use of NPs as optical labels has been advocated as an alternative to fluorescent dyes or quantum dots[17, 21-23].

NPs have been proposed as read-outs for interparticle spacing and local dielectric as their optical properties markedly depend on these parameters[5, 15, 17, 18, 24]. NPs can strongly enhance the fluorescence and photostability of nearby fluorophores and may find application in new fluorescent high-throughput detection schemes at single molecule level [22, 25, 26]. All these properties in combination with their electrical conductivity make NPs suitable for possible applications as electrically conducting links in optical biosensors[27, 28].

Fluorescence enhancement by NPs and their application in biotechnology is a relatively new subject [3, 4, 6, 12, 13, 15, 20]. Fluorophores can be described as oscillating point dipoles and when the fluorophore is localized near a metal surface, its oscillator strength and, therefore, its fluorescence can be enhanced [29-31]. Three different near-field interactions between the fluorophore and the NP have to be taken into account in the description of this

phenomenon [3, 5, 20, 21, 32-36]. Firstly, the *excitation rate* can be enhanced due to an increase of the oscillating electromagnetic field strength close to the nanoparticle. Secondly, in a similar way the *radiative rate* of the excited fluorophore can be increased. And, finally, the fluorescence may be *quenched* by energy transfer from the excited fluorophore to the conduction electrons in the NP. Depending on which term is dominant the fluorescence may be enhanced or decreased [3-5, 11, 12, 20]. It has proven difficult in the past to obtain reliable quantitative measurements of the fluorescence enhancement effect, especially at distances below a few nm from the NP surface[3, 12] and widely different fluorescence dynamics have been reported for dye-NP systems [3, 6, 12, 37, 38].

Here, the effect of nanoparticle size (ranging from 1.4 to 80 nm) on the fluorescence of an attached (fluorescently labeled) azurin molecule is investigated. Azurin (Az) from *Pseudomona aeruginosa* is a so-called blue copper protein, that contains a Cu-ion as a redox-cofactor. For most of the present experiments zinc azurin is employed in which the Cu has been replaced by Zn. Zn has only one stable oxidation state, Zn^{2+}, so that the fluorescence of the attached label is not affected by redox state changes that might complicate analysis of the experiments. By measuring the fluorescence intensity and lifetime of single dye-labeled ZnAz molecules, the effects of excitation enhancement and fluorescence quenching have been established.

To study the effect of the redox state on the fluorescence intensity and lifetime CuAz has been employed. The Cu in the azurin may occur in the Cu^+ or Cu^{2+} oxidation state. In the latter state the protein is dark blue due to a strong absorption around 625 nm whereas in the former state it is colourless. As the 625 nm absorption may give rise to Förster resonant energy transfer (FRET) from an attached dye label to the Cu, a switch in the redox state of azurin may lead to a change in fluorescence intensity of the dye. (It should be noted that the Cu centre itself is non-luminescent.) In the present study the redox state of azurin was monitored through fluorescence detection. Attachment of the protein to an 1.4 nm nanoparticle resulted in an enhanced S/N ratio. This shows that the application of nanoparticles can be used for single-molecule redox-state sensing and may offer a viable route to optically detected single-protein electrochemistry [39-47].

2. Experimental methods

Protein labeling. Azurin N42C was obtained and purified according to literature methods [39, 48]. For dye labeling the NHS-ester of Atto-647N (ATTO-TEC GmbH, Germany) was coupled to the N-terminus of either copper or zinc azurin (N42C) according to the manufacturer's instructions. Unbound label was removed using centri-spin 10 size-exclusion chromatography spin columns with a 5-kDa cut-off (Princeton Separations;

Adelphia, NJ, USA). The degree of labeling usually amounted to around 16%. Labeled protein was diluted with 20 mM Hepes buffer, pH 7.0, with final concentrations determined by UV-vis spectroscopy.

Sample preparation. The samples for fluorescence and photothermal imaging were prepared by spin coating a solution of citric-acid coated gold nanoparticles (BB International, UK; NP sizes of 10, 20, 40 or 80 nm) onto glass cover slips modified with 3-aminopropyltrimethoxysilane (APTS). The dilution and spinning speed were chosen such that the spheres were uniformly distributed over the surface (*vide infra*)[49-51]. Then 200 µL of a 50 pM of labeled Atto647N-azurin solution was applied on the coated slide and left at 4°C for 12 h. This was sufficient for obtaining strong adsorption of Az on the NPs. The slides were then washed multiple times with Hepes buffer (20mM, pH 7). The resulting azurin-gold nanoparticle constructs (Az-AuNPs) on coated glass slides were used for fluorescence measurements (see Figure 1).
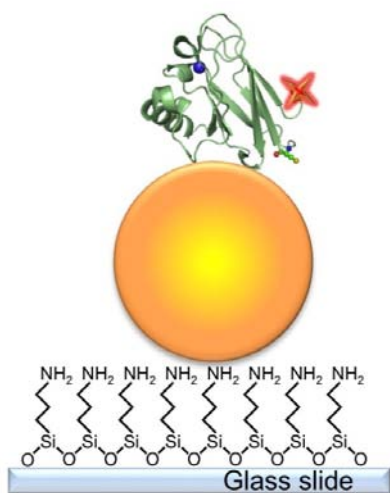
Figure 1: A schematic representation of Atto647N-labeled azurin adsorbed to AuNPs on a glass slide modified with APTS. The protein framework is depicted in green, the Cu atom in blue and the dye label in red.

For the immobilization of the azurin on 1.4 nm AuNPs a slightly different procedure was followed. The AuNPs were commercially obtained as mono-sulfo-NHS–nanogold conjugates and labeling of the azurin with these particles was performed in Hepes buffer (20 mM, pH 7) following the manufacturers protocol (Nanoprobes, USA). Subsequently, a 100 pM solution of the Az-AuNP conjugate was incubated overnight on APTS-modified

glass slides at 4ºC. The slides were subsequently washed multiple times. Measurements were performed in the same 20 mM Hepes buffer.

Control measurements were performed on azurin immobilized on *glass* and on sputtered *gold films*. *Glass slides* were cleaned by sonication in acetone, rinsed in distilled water, sonicated in aqua regia, rinsed again with water, and stored in methanol. Right before use they were dried in a stream of air and cleaned in an ozone cleaner. ATTO 647N-labeled N42C azurin was immobilized on a cleaned glass slide in high purity agarose IV (Sigma) with a gel point of 36 ± 1.5 °C. The agarose (1 %) was melted in 20 mm HEPES pH 7.0 and cooled to 50 °C. N42C azurin was added to give a final labeled protein concentration of 0.3 nM. 20 µl of azurin-containing agarose was spin-coated onto a cleaned glass slide at 2000 rpm for 10 sec yielding a thin layer of gel. The coated glass was rapidly put into a holder and covered with 1ml of 20 mm HEPES pH 7.0.

For the preparation of the 50 nm *Au films*, first a 1 nm thick adhesion layer of molybdenum-germanium (MoGe) was prepared by depositing MoGe onto a freshly cleaned glass slide through magnetron sputtering using an ATC 1800-F system (AJA corporation) at a deposition rate of 1.32 nm/min (10 mTorr Argon environment). Subsequently, gold was sputtered at a deposition rate of 9.06 nm/min (10 mTorr environment composed of a mixture of argon and 1% oxygen) on top of the MoGe film. The Au films were used immediately after preparation. Azurin (200 pM solution in 20 mM Hepes, pH 7) was immobilized directly on the bare Au films by aspecific absorption. After incubation for a few minutes, unbound azurin was washed off with buffer solution (20 mM HEPES pH 7) and the slides were used directly for measurements.

Absorption spectroscopy. Absorption spectra were measured on a Perkin-Elmer Instruments Lambda 800 spectrophotometer with a spectral bandwidth of 2 nm.

Confocal microscopy. Single-molecule fluorescence studies were performed with a home-built scanning confocal microscope equipped with Time-Correlated Single-Photon Counting (TCSPC) capabilities. For fluorescence excitation the output of a 40 MHz pulsed picosecond diode laser (PDL 800-B, PicoQuant GmbH, output wavelength: 639 nm) was sent through a narrow band clean-up filter (LD01-640/8-25, Semrock, USA), coupled into a single-mode fiber, reflected by a dichroic mirror (Z 532/633 M, Chroma technology, USA) to a high numerical aperture oil objective (100× oil, NA 1.4, Zeiss, Germany) and focused to a diffraction-limited spot (~300 nm) on the sample surface. The power density at the sample was 0.5-1 kW/cm^2. Epi-fluorescence from the labeled azurin was filtered with a band filter (D 675/50 M, Chroma technology, USA) and focused with a +45 mm focal length achromatic lens on the active area of a single photon avalanche photodiode (Perkin-Elmer SPCM-AQR-14). The data acquisition was done by the TimeHarp 200 TCSPC PC-

board operating in the special Time-Tagged Time-Resolved (T3R) mode, which stores each individual photon event without on-line data reduction [52]. Samples were mounted onto a P-517 nanopositioner (Physik Instrumente, GmbH) which was driven by an E-710 PZT controller (Physik Instrumente, GmbH). Scanning, accurate positioning, data collection and analysis were performed with the help of Picoquant SymPhoTime software (PicoQuant GmbH).

Fluorescence lifetime images were obtained by scanning a 15x15 µm^2 area of the sample with a step size of 100 nm and a dwell time of 3 ms per pixel. To accurately determine the fluorescence lifetimes of immobilized labeled Cu-azurin in the reduced and in the oxidized state, photon decay histograms of the photons collected over the whole image were constructed. Lifetimes for individual particles were obtained from the photon decay histograms recorded by placing the laser excitation spot on the individual particles. Deconvolution with the instrumental response function (IRF) and a fit to a bi-exponential decay was carried out by using the SymPhoTime software.

Photothermal imaging setup. A photothermal imaging setup was used as described earlier in detail [53]. Briefly, it was based on an inverted microscope (Olympus IX71) which was equipped with an oil immersion objective (60x, NA = 1.45, Olympus,). The heating beam was provided by an Ar-ion laser (Coherent) at 514 nm. The heating light passed an acousto-optical modulator (AOM) which also sent a reference signal to a lock-in detector (SR844, Stanford Research Systems). The probe beam at 790 nm was provided by a Ti:sapphire laser (3900S, Spectra Physics, pumped by 90% of the power of the Ar-ion laser). Both beams were expanded to diameters of about 20 mm to overfill the entrance pupil of the microscope objective (approximately 10 mm), and were combined on a dichroic mirror (BS 669, AHF).

The back/scattered probe light returned from the sample, passed the dichroic mirror, and was directed by a 50/50 beam splitter (Halle) towards a clean-up interference filter (Omega) and a Si photodiode (DHPCA-100-F, Femto). Optionally the probe beam was monitored by a CCD camera (Ganz).

The photodiode provided the signal for demodulation of the photothermal response with the lock-in amplifier, while the sample was scanned with a 3-axis piezostage (MARS, Physik Instrumente). Data acquisition and processing were controlled by an acquisition card (ADWin Gold) linked to a computer.

3. Results

## 3.1 Optical characterization of Az-AuNPs in solution.

The bulk solution optical properties of the Au colloids were recorded prior to use in the single-molecule study. Figure 2 presents the absorption spectra, which exhibit the characteristic surface plasmon peaks of the AuNPs. The excitation maxima undergo a red shift from 519 to 540 nm as the particle diameter increases from 10 to 80 nm, illustrating the wavelength dependence of the surface plasmon resonance (SPR) on particle size [54]. The peak widths are also observed to increase with particle diameter.

The influence of Az binding on the absorption spectrum of a AuNP solution is shown in Figure 3 for several concentrations (0, 5µM, 10 µM and 50 µM) of CuAz in a buffered (20 mM HEPES pH 7) solution of 80 nm AuNPs. The absorption spectrum of Cu azurin [55] shows two main peaks at 280 nm and 628 nm. The latter peak only appears in the oxidized form [55]. The spectra in Figure 3 are dominated by the AuNP SPR absorption, with a small contribution around 625 nm from azurin (the spectra were not corrected for free azurin present in solution), as the extinction coefficient of the AuNP (around 10^8 - 10^{11} M^{-1} cm^{-1} depending on particle size [16, 54]) is much higher than that of Az (5700 $M^{-1}cm^{-1}$ at 625 nm) [55]. The red shift and the width of the SPR band increase as the Az concentration increases
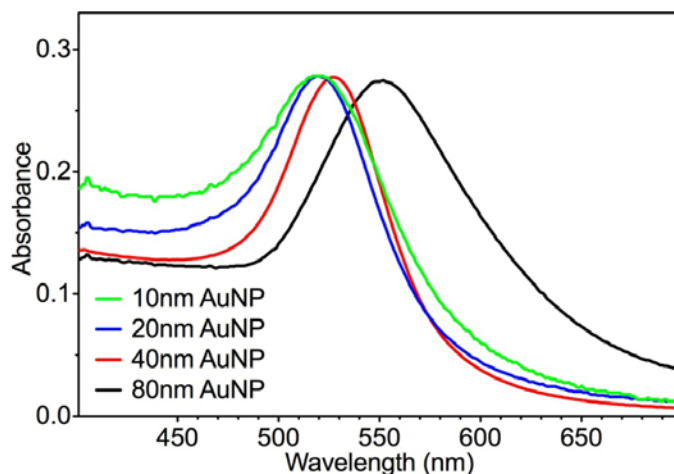
Figure 2: Absorption spectra of four sizes of Au nanoparticles in solution normalized at the peak height in the 500-600 nm region. The solutions were prepared as 1:1 dilutions from the solutions obtained from the manufacturer. Spectra taken in Millipore water at ambient temperature. Particle sizes (as indicated by the colors in the graph): 10, 20, 40 and 80 nm. Spectra are normalized with respect to their absorption maxima. Absorbance in arbitrary units.

(Figure 3, inset) corresponding to an increase in the amount of surface immobilized Az. This suggests that a single AuNP can bind several Az molecules, in line with the facile binding between Az and AuNPs observed previously [51]. The shift is ascribed to the protein-induced change in local dielectric environment of the AuNPs [56-58]. The largest shift amounts to about 5 nm at the highest Az concentration (50 μM)
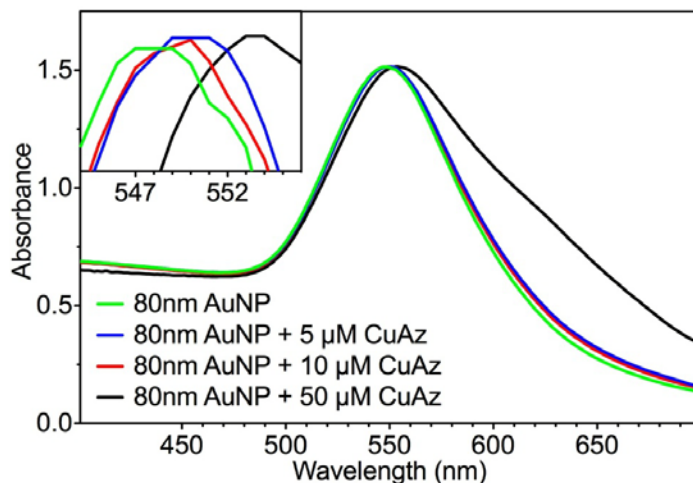
Figure 3: Absorption spectra of a AuNP (80nm diameter) solution (20 mM Hepes, pH 7) in the presence of various amounts of CuAz : 0μM (green), 5μM (blue), 10μM (red) and 50μM (black). The spectra are normalized on the height of the peak around 550 nm. Inset: zoom of the SPR bands showing up to 5nm peak shifts to higher wavelengths with the Az concentration increasing from 5 to 50μM (0, 5, 10 and 50μM). Absorbance in arbitrary units.

The maximum number of Az molecules that can bind to a single AuNP was estimated at 1700 /NP corresponding with a close and uniform Az layer around the NP[‡]. In our case the number of Az molecules in solution is larger than what is needed to form a monolayer on the NP. Thus, because the number of Az bound to the NP still depends on the concentration under excess Az conditions, we conclude that the theoretical maximum is not reached, and

---

[‡] The number of Az molecules that can ultimately bind to a single AuNP depends on the size of the protein and the NP size. The theoretical number of Az molecules that can be packed around a spherical NP, N_{Az}, can be estimated by [50,56]: $N_{Az} = 0.65(R_T^3 - R_{NP}^3) / R_{Az}^3$ [1]

where R_{NP} is the radius of the NP (40 nm), R_{Az} is the azurin radius (2 nm, assuming a quasi-spherical shape [59], and R_T is the radius of the AuNP plus bound Az molecules ($R_{NP}+2R_{Az}$).

that an equilibrium between free and bound azurin sets in at sub-monolayer coverage of the NP. In the single-molecule studies, we took special care to ensure the binding of only one labeled azurin per NP (*vide infra*).

3.2 Fluorescence images and time traces

Photothermal microscopy was applied to verify that AuNPs were bound as single particles without clustering. Figure 4A shows a photothermal image of a sample with 40 nm diameter gold NPs immobilized on top of an APTS modified glass slide in water. The distribution of photothermal signals is monodisperse and well-offset from the background (Fig. 4B). These results confirm the effectiveness of the protocol used for preparation of samples of single particles bound to the glass surface without clustering, since the photothermal signal is proportional to the absorption-cross section of NPs and thus to the third power of NP diameter. Similar results (not shown) were obtained for 10, 20 and 80 nm diameter AuNPs.

The intrinsic luminescence signal from individual AuNPs occurs at the same wave length as the excitation light while the fluorescence of labeled Az molecules occurs at longer wave lengths. Thus the Az-modified AuNPs can be easily separated from unmodified ones. We also keep the fluorescence excitation power low in our experiments to avoid saturation effects and possible modification of intrinsic fluorescence properties of AuNPs [8].
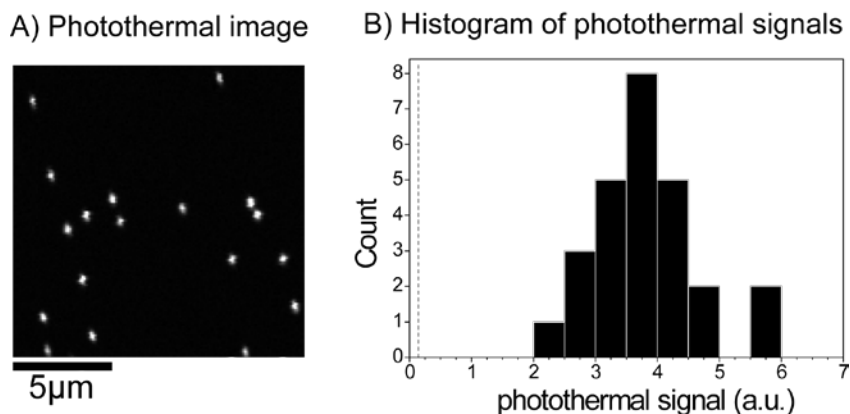
Figure 4. A) (A) Photothermal image of individual 40 nm diameter AuNPs spin-coated on an APTS-modified glass surface. Particles are well-separated from each other. (B) Histogram of photothermal signals from several images obtained at the same experimental conditions. Vertical dashed line indicates signal background level. The monodisperse character of the distribution and its clear off-set from the background is a clear indication for the absence of aggregates.

To investigate the effect of NP size on the fluorescence intensity, confocal images (Figure 5A) were recorded for labeled Zn-Az immobilized on AuNPs ranging in size from 1.4 to 80 nm. Control measurements were performed for Zn-Az immobilized on glass and on flat gold (Figure 5A). Well-separated bright spots derive from single Az molecules. A big variation in peak intensity among the different images is immediately evident from the scale bars (compare f.i. in Figure 5A the panel 'ZnAz on glass' (maximum count number of 120) with the panel '10 nm AuNP-ZnAz' (maximum count number of 1415)). Compared to ZnAz on glass the fluorescence emission from Atto-647N-labeled ZnAz increases significantly when the protein is bound to 1.4 nm AuNPs and the intensity keeps increasing with the size of the AuNPs (see Figure 5, panels B and C). By contrast, labeled Zn-Az which is deposited directly onto a 50 nm thick gold film experiences fluorescence *quenching* instead of *enhancement* (see Figure 5). The images show some heterogeneity in the fluorescence intensity, which is ascribed to variation in protein orientation leading to
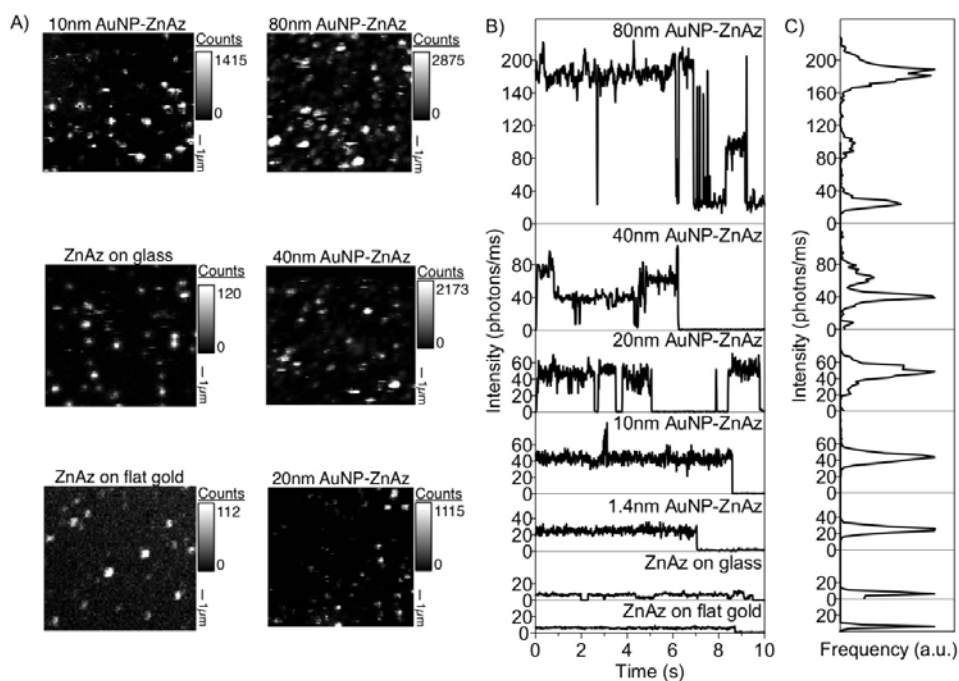
Figure 5: A). Confocal images (15×15 μm, step size 100 nm, dwell time 3 ms/pixel) of labeled Zn-azurin bound to AuNPs, labeled Zn-azurin on flat gold and labeled Zn-azurin on an APTS-modified glass side. Scale bar shows the intensity counts in 3 msec bins. B) Time traces of individual azurin molecules on 50 nm thick flat gold, APTS-modified glass and AuNPs. C) Count rate histograms corresponding to the traces in panel B.

74

variation in the fluorophore-NP distance and the fluorophore orientation.

Typical intensity time traces of single Az molecules attached to all of the five AuNPs used in this study (1.4, 10, 20, 40, and 80 nm) and of Az molecules on glass and flat Au are presented in Figure 5B. From the observed single-step bleaching in the Az-AuNP fluorescence time traces (Figure 5B, discussed in more detail below), we conclude that at most a single fluorescent azurin is bound per nanoparticle. As already seen in Figure 5A, compared to Az immobilized on a glass surface the fluorescence intensities increase significantly with AuNP size, from a 3-fold enhancement for the 1.4 nm AuNPs up to 29-fold for Az bound to an 80 nm AuNP. The enhancement factors have been collected in Table 1, 2nd column (vide infra).
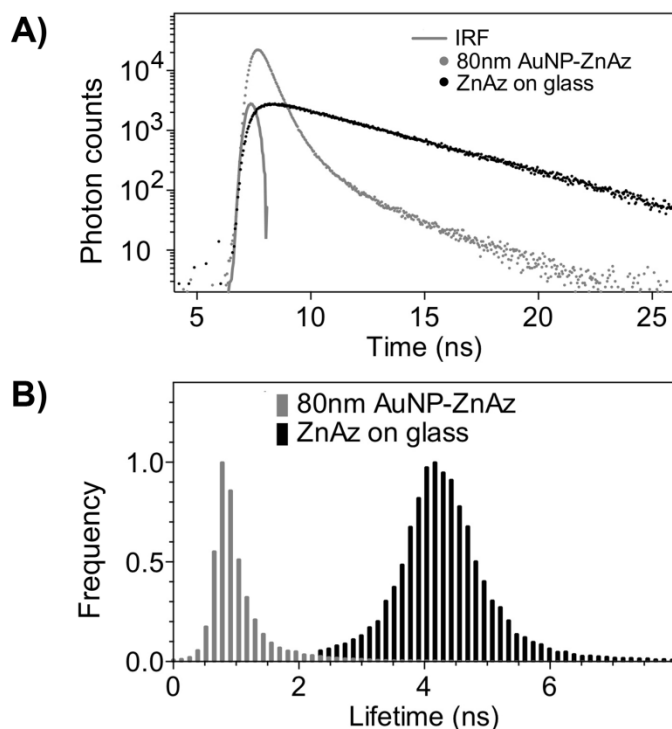

Figure 6: A). Typical TCSPC decay curves of single Zn azurin molecules on an APTS-modified glass slide (black dots) and on an AuNP of 80nm diameter (light gray dots). The light gray line shows the instrument response function (IRF). B). Normalized histograms of lifetimes of single azurin molecules (data taken from over 150 molecules) on glass (black) and AuNP 80 nm diameter (light gray).

3.3 Lifetime measurements and fluorescence enhancement

To provide further insight into the fluorophore-nanoparticle interaction fluorescence lifetime studies were carried out on the conjugate Az-AuNPs. As an example the fluorescence intensity decay of labeled Zn-Az attached to an 80 nm AuNP is shown in Figure 6A. A bi-exponential decay model with a main component (amplitude = 0.96) and a lifetime τ = 0.85 ns, and a minor component with τ = 2.4 ns describes well the experimental decay histograms. Figure 6B shows histograms of the lifetimes estimated from fluorescence decays of more than 150 individual molecules.

The fluorescence lifetime distributions of Zn-Az are plotted for all NP sizes in Figure 7 together with the flat-gold and glass distributions. A dramatic decrease in the lifetime with increasing particle size is observed, with the lifetime changing from 3.5 to 0.85 ns for NP sizes going up from 1.4 to 80 nm (see also Table 1, 3rd column). Some of the lifetime distributions are somewhat asymmetric with a tail towards longer lifetimes. For the NPs we ascribe this to variation in fluorophore-NP distance and orientation. The long-lifetime tail which is noticeable in the Az-on-glass distribution is attributed to the background, which is relatively strong for the non-enhanced signal of Az on glass.
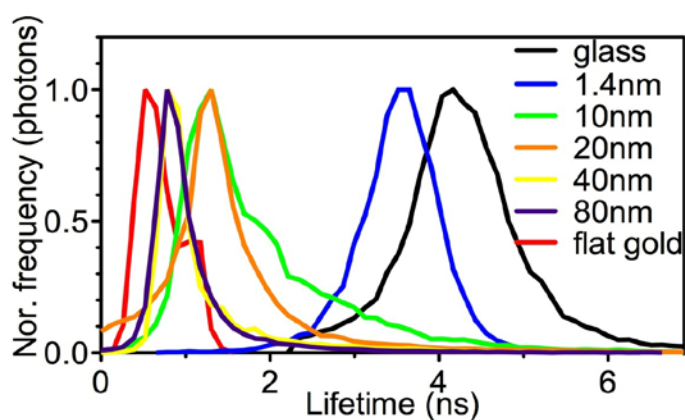
Figure 7: Lifetime histograms of Atto647N-labeled single Zn-azurin molecules immobilized on a glass surface, on a 50 nm thick flat gold film and on AuNPs of varying size (1.4, 10, 20, 40 and 80 nm).

3.4 Single-molecule redox state detection

We checked whether the FRET-based fluorescence detection method [39, 40] can be applied to the observation of the redox state changes of single Cu-Az molecules bound to AuNPs. Oxidizing (K_3 [Fe $(CN)_6$]) and reducing (sodium ascorbate) reagents were used to change the redox state of the protein. Time traces and TCSPC decay curves of Atto647N-labeled Cu-Az bound to 1.4 nm AuNPs are shown in Figures 8A and B, respectively. The ratio between reduced (Figure 8A, top trace) and oxidized (Figure 8A, bottom trace) intensities is about 4. The excited state lifetimes are 3.5 ns and 1.4 ns for reduced and oxidized azurin, respectively. As expected, the reduced Az lifetime is the same as for the redox-inactive Zn-Az bound to this NP. The decay of oxidized Az had to be fitted to a bi-exponential model,
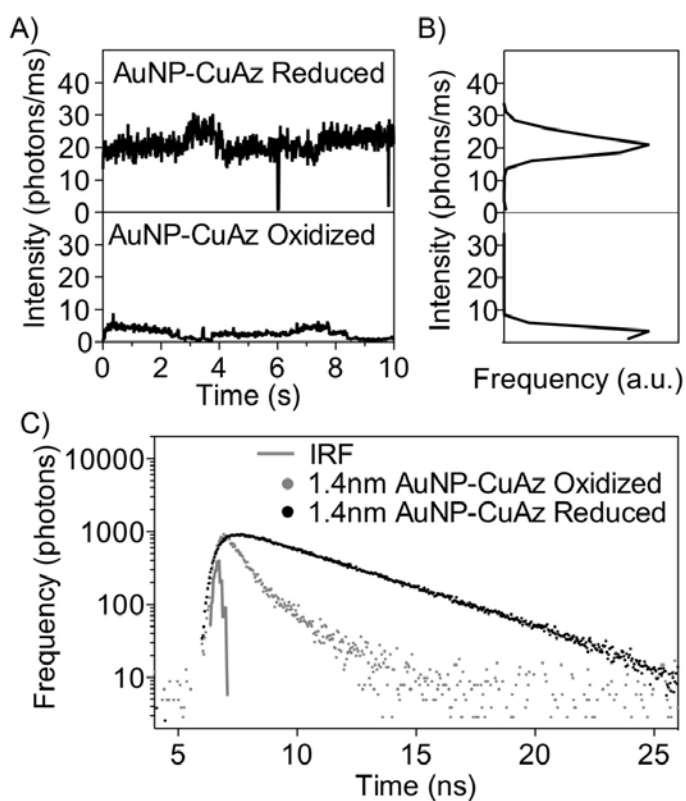
Figure 8: A) Time traces, B) intensity histograms and C) TCSPC decay curves of individual A647N-labeled Az (Cu-Az) proteins bound to 1.4 nm AuNP in reduced and oxidized states. Best fits for the decay curves were 3.5 ns for the reduced form and 1.4 ns for the oxidized form. The TCSPC curve of the instrument response function (IRF) is also included (panel C light gray line).

with 1.4 ns the dominant lifetime and a relative amplitude of more than 90%. The second component had a lifetime of 0.5 ns and an amplitude of less than 10%, and was attributed to the background. Thus, the redox activity can be measured down to single molecule level. Attachment to the AuNP is responsible for enhanced fluorescence and, thereby, for enhanced sensitivity.

We find the intensity-based switching ratio, Q_I, to be 0.75 with

$$Q_I = 1 - (F_{oxid} / F_{red}) \ . \tag{2}$$

Here, F_{oxid} and F_{red} denote the fluorescence intensity of the Az in the reduced and oxidized form, respectively [40]. The lifetime-based switching ratio [60] is given by Q_L with:

$$Q_L = 1 - (\tau_{oxid} / \tau_{red}) \ . \tag{3}$$

Here, τ_{oxid} and τ_{red} denote the fluorescence lifetime of the Az in the reduced and oxidized form, respectively. Q_L is found to be around 0.6, slightly lower than the intensity-based value. A much more pronounced discrepancy between Q_I and Q_L was found for Atto655-labeled Az immobilized on gold films [61] with $Q_I = 0.7$ and $Q_L = 0.4$. This discrepancy may be due to dye-specific photophysics and is currently subject of further investigation.

4. Discussion

From the results presented above, it is clear that immobilization of a dye-labeled protein onto a nanoparticle may have a pronounced effect on the fluorescence of the protein-dye construct. Enhancement of the emission intensity and shortening of the fluorescence lifetime occur simultaneously, and both effects increase monotonously with increasing NP size. The combination of intensity enhancement and lifetime shortening has been demonstrated previously for fluorophore-nanoparticle combinations [1, 3, 4, 6, 12, 20, 62] and for fluorophores immobilized on several types of metal film[13, 61, 63-65].

It is of interest to compare our observations to these reports in more detail. Enhancement factors ranging from 8 to 13 have been reported for single dye molecules close to 80 nm and 100 nm AuNPs [3, 4, 12, 20]. In the present case we see an enhancement by a factor of 29 for 80 nm AuNPs. Several factors may account for this difference: firstly, previous values were taken from confocal images rather than time traces. Values from images will be an average over bright and dark phases if blinking is present, whereas in our experiments only the bright phases were taken into account. Secondly, the enhancement is strongly dye-dependent and in previous studies other dyes were used than the one employed in the present study [66]. Thirdly, the fluorophore-metal interaction may also be enhanced by the dielectric medium. It was shown by Härtling et al. [5] that a medium with an intermediate

refractive index such as water, will result in a larger enhancement than when air or a higher-refractive index medium such as immersion oil, is used. Water is the medium used in our experiments, whereas in most previous single-molecule studies [3, 4, 12, 20] the medium was a spin-coated film of PMMA or para-terphenyl, both with a rather higher refractive index than water. There is a report by Fu et al. [6] in which water is used with NP-dye constructs in solution, showing an intensity enhancement factor of 15, but the dye-NP distance is rather longer than ours and silver NPs are used, so that the results are not directly comparable.

Results of <u>lifetime measurements</u> can be compared to a few literature reports. Kühn et al. [3] observe a 20-fold lifetime reduction together with a 13-fold intensity enhancement for a terrylene dye at 2 nm distance of a 100 nm AuNP. Fu et al. [6] report a 15-fold enhancement of Cy5 fluorescence for a distance of 8 nm between the dye and a 50 nm AgNP; the Cy5 lifetime is shortened from 2.3 to 0.43 ns. A similar result is obtained by Fu and Lakowicz for Cy5 on silver island films [65]. These three studies thus show similar combinations of intensity enhancement and lifetime shortening as we report. For SAMSA, a fluorescein derived dye, on 5 to 20 nm size AuNPs, a reduction in both intensity and lifetime (compared to the free-dye case) is observed by Cannone et al. [2], presumably because of the small size of the NPs. Most measurements of lifetime shortening were carried out on ensembles of fluorophores, which, moreover, were mostly immobilized on silver and gold island films or particle films [31, 62-64, 67]. Hence, these results are not fully comparable to ours. Although combinations of intensity enhancement and lifetime shortening were reported similar to the results of the present study, the absolute values are less unequivocal as the data may have been averaged over a heterogeneous population while also concentration differences between experiments cannot be excluded.

A <u>more quantitative analysis</u> of our data is based on previously developed theoretical models of fluorophore-metal interactions [12, 20, 21, 33-36]. The fluorescence rate (γ_{em}) of a single molecule can be expressed as [12, 20]:

$$\gamma_{em} = \gamma_{exc} q \tag{4}$$

with γ_{exc} and q the excitation rate and quantum yield respectively. For a free molecule in solution the quantum yield is denoted as q_0, which takes the form

$$q_0 = \frac{\gamma_{r,0}}{\gamma_{r,0} + \gamma_{nr.0}} = \gamma_{r,0}\tau_0 \tag{5}$$

with $\gamma_{r,0}$ and $\gamma_{nr,0}$ the (free-space) radiative and nonradiative decay rate, respectively, and τ_0 is the fluorescence lifetime of the free molecule. The presence of metal particles will lead

to a change in the quantum yield in two ways. The radiative decay may be enhanced by coupling of the excited state dipole into the locally modified electromagnetic field, and the nonradiative decay may increase due to quenching by energy transfer from the fluorophore to the metal. In the expression for the quantum yield this is incorporated by taking γ_r to be variable, and by introducing an additional quenching ('energy absorption') rate γ_{abs}; the nonradiative decay rate γ_{nr} is taken to be intrinsic, *i.e.*, $\gamma_{nr} = \gamma_{nr,0}$ [4, 12, 31]. This gives:

$$q = \frac{\gamma_r}{\gamma_r + \gamma_{nr.0} + \gamma_{abs}} = \gamma_r \tau \qquad [6]$$

The lifetime of a fluorophore-metal system is also modified by the change in γ_r and the additional decay rate, γ_{abs}, and is given by

$$\tau = (\gamma_r + \gamma_{nr,0} + \gamma_{abs})^{-1} \qquad [7]$$

If the enhancement of the radiative rate dominates over the quenching effect, the quantum yield may increase in the vicinity of a metal NP. The largest attainable value of *q* is 1 [3-5, 12, 20, 21, 66].

More commonly, it is assumed that γ_{exc} is strongly enhanced in the vicinity of a NP. For weak excitation (below saturation) which is applicable here, the excitation rate is proportional to $|\mathbf{E} \cdot \mathbf{p}|^2$, with *E* the local electric field and *p* the transition dipole moment [5, 12, 20]. Therefore, the highly enhanced local electromagnetic field near a AuNP can effectively increase the excitation rate. The net enhancement is, therefore, a composite result of excitation enhancement, radiative rate enhancement and increased quenching. All of these terms depend on the metal particle properties and on the distance between the fluorophore and the NPs. In the sub-5 nm regime of Az-NP distances, the radiative rate enhancement is usually calculated to be small compared to the other two effects [12, 20].

From our data we can estimate the magnitude of the three effects using fluorescence intensity and lifetime information (Table 1). Taking the results on the glass surface to correspond to the free molecule quantities $\gamma_{em,0}$, $\gamma_{exc,0}$ and q_0, we obtain [20]:

$$\frac{\gamma_{em}}{\gamma_{em,0}} = \frac{\gamma_{exc}}{\gamma_{exc,0}} \frac{q}{q_0} \qquad [8]$$

We calculate $\gamma_{exc}/\gamma_{exc,0}$ for two limiting cases. In the *'quenching limit'*, we assume the radiative rate change is negligible. This implies that the change in quantum yield is proportional to the change in lifetime:

$$\frac{q}{q_0} = \frac{\tau}{\tau_0}$$

[9]

which gives

$$\frac{\gamma_{exc}}{\gamma_{exc,0}} = \frac{\gamma_{em}}{\gamma_{em,0}} \frac{\tau}{\tau_0}$$

[10]

with the enhancement of γ_{em} equal to the increase in intensity observed in the fluorescence time traces (Figure 6B). The resulting values for the excitation enhancement ($\gamma_{exc}/\gamma_{exc,0}$) are listed in column 4 of Table 1. It is seen that γ_{exc} increases with nanoparticle size up to 145-

Substrate	$\gamma_{em} / \gamma_{em,0}$ [b]	τ (ns) [c]	$\gamma_{exc} / \gamma_{exc,0}$ [d]	$\gamma_{exc} / \gamma_{exc,0}$ [e]
Glass	1	4.2	1	1
1.4 [a]	3	3.50 (1.45)	4	2.0
10 [a]	6	1.60 (0.95)	16	4
20 [a]	7	1.55 (0.93)	19	4.6
40 [a]	11	0.85 (0.62)	55	7.2
80 [a]	29	0.85 (0.62)	145	19
Au film [f]	0.7	0.65	7	0.4

Table 1: Fluorescence enhancement values and lifetimes for labeled Zn-azurin and Cu-azurin bound to AuNPs with different sizes. All data pertain to Zn-azurin except the data in parentheses in column three, which refer to oxidized Cu-azurin. Calculations for Zn-azurin are based on equations [8]-[10].

a) Diameter of Au NP, nm.

b) Observed fluorescence rate γ_{em} (Eq. [4]) normalized to the rate measured for Atto647N-labeled ZnAz on glass in the absence of NPs. Fluorescence rates are taken from the peak value of the count rate histograms of the intensity time traces (Fig. 5B). Note that these values reflect only the bright parts of the traces, i.e. the effect of blinking is not included.

c) Fluorescence lifetime, as obtained from TCSPC decay curves (Figs 6 and 7). The data in parentheses refer to oxidized Cu-azurin. See text for further details on the Cu-azurin data.

d) Calculated excitation rate γ_{exc} (using Eq. 10]) normalized to the rate for Az on glass, assuming that the radiative rate γ_r is not affected by the NP, i.e., $\gamma_r = \gamma_{r,0}$ (see text for details). The lifetime τ_0 of Atto-647N-labeled Az on glass is 4.2 ns.

e) Excitation rate γ_{exc} as in c, but now under the assumption that the radiative rate is increased and the quantum yield increases from 0.65 (=q_0) to 1(=q) (see Eq. [8] and text for details).

f) Labeled Zn-azurin immobilized on a bare, 50 nm thick Au film

fold for the 80 nm NP.

The second limiting case, which we refer to as the '*radiative limit*', is based on the assumption that the radiative rate increase is large and that the lifetime shortening should be fully ascribed to radiative enhancement [31, 36, 63]. In our calculation we use this limit to the extent that q is taken to be ≤ 1. With q_0 equal to 0.65 for Atto647N (value provided by the manufacturer) and $q = 1$, we calculate the excitation rate enhancements from Equation [8] as shown in column 5 of Table 1. Again, we see an increase of the excitation enhancement with NP size, with a maximum of 19 for the 80 nm NP.

A value of 25 for the enhancement of γ_{exc} was calculated by Kühn et al. [3] for a 100 nm nanoparticle, which seems to suggest that the value of 19 found in the radiative limit is more realistic than the factor of 145 calculated above for the quenching limit. However, the relative importance of the factors found by Kühn et al. corresponds more to the 'quenching limit', as they unequivocally show that the net enhancement (*i.e.*, the increase in γ_{em}, for which they find a factor 13) is *lower* than the excitation rate (γ_{exc}) enhancement in their case (in the radiative limit, the opposite obtains with the net enhancement of 29 in our case being *higher* than the factor of 19 for γ_{exc}) and that quenching cannot be neglected. We believe this - *i.e.*, the presence of both significant quenching and excitation enhancement - to be applicable to our fluorophore-NP system as well, and expect the real values for the excitation enhancement to lie in between the two limits and above the enhancement factor for γ_{em}. Full-scale modeling of the three components is required to shed more light on this issue.

As shown above, the net enhancement of fluorescence intensity increases with nanoparticle size. Such a size effect was previously predicted [4, 5, 68]. Anger et al. [4] calculate a factor of 5 difference in the γ_{em} values of Nile blue dye molecules close to 20 and to 80 nm AuNPs, and Härtling et al. [5] calculate the effect for 30 nm and 80 nm AuNPs and find a difference of about a factor 6 between these two sizes, for configurations comparable to ours, at ~5 nm distance between dye and NP. These differences are close to the factor of 4 we see between the γ_{em} enhancements induced by 20 nm and 80 nm NPs. The *absolute* values predicted by these authors for the γ_{em} enhancements, on the other hand, are rather lower than what we observe. The 20 resp. 30 nm NPs are predicted to produce a net change of fluorescence intensity by a factor of 0.3 [4] and 0.2, respectively [5], (*i.e.*, a *decrease* in intensity) in marked contrast to the 7-fold intensity enhancement we observe for 20 nm NPs. Thus, the experimental verification provided by our study may be of help in refining the theoretical predictions.

Furthermore, we find that in the same fluorophore-metal distance regime (up to 4 nm) the fluorescence enhancement is dominant when Az is coupled to AuNPs, whereas the fluorescence of Az is quenched when it is adsorbed on a gold film (Figure 6A, bottom right). In the latter case, the interaction will be dominated by quenching, as there are more states available to which energy transfer can take place. At the same time, for gold films the roughness of the surface also has a large effect on the net intensity change [61, 62, 67, 69-73], with more enhancement for rougher films (i.e. with larger, more nanoparticle-like surface structures).

With the strong size dependence of both enhancement and quenching, it is of interest to see how far we can take the redox state detection in the vicinity of gold NPs. So far, we have measured redox switching for CuAz attached to a 1.4 nm NP only (see Figure 8). For this NP size, reduced and oxidized CuAz lifetimes are 3.5 ns and 1.4 ns respectively. We can analyze the data further by looking into the contribution of the FRET mechanism to the lifetime shortening in the Cu(II)Az form. For the reduced form it was stated (see Eq. 7) that $\tau_{red} = (\gamma_r + \gamma_{nr} + \gamma_{abs})^{-1}$. For the oxidized form the expression for the lifetime becomes $\tau_{ox} = (\gamma_r + \gamma_{nr} + \gamma_{abs} + \gamma_{FRET})^{-1}$ in which γ_{FRET} is the rate of energy transfer from the label to the Cu as a result of FRET. With τ_{red} = 3.5 ns and τ_{ox} = 1.4 ns one finds $1/\gamma_{FRET}$ = 2.33 ns. It may be assumed safely that γ_{FRET} is independent of AuNP size (the FRET phenomenon in our case is an intramolecular effect between Cu and label and has nothing to do with the label-NP interaction) and that the fluorescence lifetimes of Cu(I)Az and ZnAz (there is no FRET between label and metal in both cases) are the same it is easy to calculate τ_{ox} for the other AuNP sizes. The data are collected in Table 1, 3rd column (numbers in parentheses).

The numbers in Table 1 show that as the nanoparticle size increases the difference between τ_{red} and τ_{ox} becomes progressively smaller and more difficult to detect, therefore. This is because the increase in radiative rate makes the life times less sensitive to differences in the non-radiative rates[74]. However, the smaller difference in life times is more than compensated by the concomitant increase in fluorescence intensity which allows for higher signal to noise ratios. The net effect is a slight increase in sensitivity for detecting redox changes at the single molecule level with increasing NP size. Larger NPs, however, allow for multiple attachment of labeled protein molecules which would result in greatly enhanced sensitivity for detecting environmental changes in redox potential.

Further improvements may be obtained by applying specific immobilization strategies which give more control over the dye-AuNP distance and orientation. Changes in orientations and distances may affect the quenching and enhancement terms differently, so that obtaining an even larger intensity enhancement without a further increase in quenching

may be feasible. Even more promising might be the application of nanorods instead of spherical AuNPs ('lightning effect')[75, 76]. For electrochemical applications, the distance between redox center and metal should be within 1 or 2 nm to ensure sufficient electronic coupling between protein and electrode. Investigations into the electrochemical control of an Az-AuNP system are currently underway.

5. Conclusion

We have shown that the fluorescence of dye-labeled azurin can be enhanced by attaching the protein to a gold nanoparticle. This study demonstrates for the first time the theoretically predicted NP size dependence of fluorophore-NP interaction. In addition, the observed enhancement factors, of up to 29 times increase in intensity for Az on 80 nm AuNPs, are a huge improvement compared to previous observations. By controlling the distance and the orientation of the protein on the AuNP through a covalent link, the fluorescence enhancement may yet be further improved.

In the used AuNP-labeled protein system, the detection of the protein redox state with enhanced fluorescence intensity was shown to be feasible. The system can be easily prepared and applied to various redox proteins and biomolecules, offering new possibilities of single-molecule redox state detection as well as of high-throughput analysis.

References

1. Dulkeith E, Morteani AC, Niedereichholz T, Klar TA, Feldmann J, Levi SA, van Veggel FCJM, Reinhoudt DN, Moller M, Gittins DI. Fluorescence quenching of dye molecules near gold nanoparticles: Radiative and nonradiative effects. *Physical Review Letters* 2002; **89**(20).

2. Cannone F, Chirico G, Bizzarri AR, Cannistraro S. Quenching and blinking of fluorescence of a single dye molecule bound to gold nanoparticles. *Journal of Physical Chemistry B* 2006; **110**(33):16491-16498.

3. Kuhn S, Hakanson U, Rogobete L, Sandoghdar V. Enhancement of single-molecule fluorescence using a gold nanoparticle as an optical nanoantenna. *Physical Review Letters* 2006; **97**(1).

4. Anger P, Bharadwaj P, Novotny L. Enhancement and quenching of single-molecule fluorescence. *Physical Review Letters* 2006; **96**(11).

5. Hartling T, Reichenbach P, Eng LM. Near-field coupling of a single fluorescent molecule and a spherical gold nanoparticle. *Optics Express* 2007; **15**(20):12806-12817.

6   Fu Y, Zhang J, Lakowicz JR. Plasmonic enhancement of single-molecule fluorescence near a silver nanoparticle. *Journal of Fluorescence* 2007; **17**(6):811-816.

7. Gaiduk A, Yorulmaz M, Orrit M. Correlated Absorption and Photoluminescence of Single Gold Nanoparticles. *Chemphyschem* 2011; **12**(8):1536-1541.

8 Gaiduk A, Ruijgrok PV, Yorulmaz M, Orrit M. Making gold nanoparticles fluorescent for simultaneous absorption and fluorescence detection on the single particle level. *Physical Chemistry Chemical Physics* 2011; **13**(1):149-153.

9. Yun CS, Javier A, Jennings T, Fisher M, Hira S, Peterson S, Hopkins B, Reich NO, Strouse GF. Nanometal surface energy transfer in optical rulers, breaking the FRET barrier. *Journal of the American Chemical Society* 2005; **127**(9):3115-3119.

10. Chhabra R, Sharma J, Wang HN, Zou SL, Lin S, Yan H, Lindsay S, Liu Y. Distance-dependent interactions between gold nanoparticles and fluorescent molecules with DNA as tunable spacers. *Nanotechnology* 2009; **20**(48).

11. Taminiau TH, Stefani FD, Segerink FB, Van Hulst NF. Optical antennas direct single-molecule emission. *Nature Photonics* 2008; **2**(4):234-237.

12. Bharadwaj P, Anger P, Novotny L. Nanoplasmonic enhancement of single-molecule fluorescence. *Nanotechnology* 2007; **18**(4).

13. Fu Y, Lakowicz JR. Modification of single molecule fluorescence near metallic nanostructures. *Laser & Photonics Reviews* 2009; **3**(1-2):221-232.

14. Fort E, Gresillon S. Surface enhanced fluorescence. *Journal of Physics D-Applied Physics* 2008; **41**(1).

15. Lakowicz JR. Plasmonics in biology and plasmon-controlled fluorescence. *Plasmonics* 2006; **1**(1):5-33.

16. Liu XO, Atwater M, Wang JH, Huo Q. Extinction coefficient of gold nanoparticles with different sizes and different capping ligands. *Colloids and Surfaces B-Biointerfaces* 2007; **58**(1):3-7.

17. Pelton M, Aizpurua J, Bryant G. Metal-nanoparticle plasmonics. *Laser & Photonics Reviews* 2008; **2**(3):136-159.

18. Barnes WL. Fluorescence near interfaces: the role of photonic mode density. *Journal of Modern Optics* 1998; **45**(4):661-699.

19. Girard C. Near fields in nanostructures. *Reports on Progress in Physics* 2005; **68**(8):1883-1933.

20. Bharadwaj P, Novotny L. Spectral dependence of single molecule fluorescence enhancement. *Optics Express* 2007; **15**(21):14266-14274.

21. Bharadwaj P, Deutsch B, Novotny L. Optical Antennas. Advances in Optics and Photonics. *Optics and Photonics* 2009; **1**:438-483.

22. Anker JN, Hall WP, Lyandres O, Shah NC, Zhao J, Van Duyne RP. Biosensing with plasmonic nanosensors. *Nature Materials* 2008; **7**(6):442-453.

23. Salata OV. Applications of nanoparticles in biology and medicine. *Journal of Nanobiotechnology* 2004; **2**:3-8.

24. Zhang J, Fu Y, Chowdhury MH, Lakowicz JR. Single-molecule studies on fluorescently labeled silver particles: Effects of particle size. *Journal of Physical Chemistry C* 2008; **112**(1):18-26.

25. Sanvicens N, Pastells C, Pascual N, Marco MP. Nanoparticle-based biosensors for detection of pathogenic bacteria. *Trac-Trends in Analytical Chemistry* 2009; **28**(11):1243-1252.

26. Li YY, Schluesener HJ, Xu SQ. Gold nanoparticle-based biosensors. *Gold Bulletin* 2010; **43**(1):29-41.

27. Katz E, Willner I. Integrated nanoparticle-biomolecule hybrid systems: Synthesis, properties, and applications. *Angewandte Chemie-International Edition* 2004; **43**(45):6042-6108.

28. Willner I, Willner B, Katz E. Biomolecule-nanoparticle hybrid systems for bioelectronic applications. *Bioelectrochemistry* 2007; **70**(1):2-11.

29. Zhang J, Fu Y, Chowdhury MH, Lakowicz JR. Enhanced Forster resonance energy transfer on single metal particle. 2. Dependence on donor-acceptor separation distance, particle size, and distance from metal surface. *Journal of Physical Chemistry C* 2007; **111**(32):11784-11792.

30. Lakowicz JR. Radiative decay engineering: Biophysical and biomedical applications. *Analytical Biochemistry* 2001; **298**(1):1-24.

31. Zhang YX, Aslan K, Previte MJR, Geddes CD. Metal-enhanced fluorescence from copper substrates. *Applied Physics Letters* 2007; **90**(17).

32. Waldeck DH, Alivisatos AP, Harris CB. Nonradiative Damping of Molecular Electronic Excited-States by Metal-Surfaces. *Surface Science* 1985; **158**(1-3):103-125.

33. Chance RR, Prock A, Silbey R. Comments on Classical-Theory of Energy-Transfer .2. Extension to Higher Multipoles and Anisotropic Media. *Journal of Chemical Physics* 1976; **65**(7):2527-2531.

34. Chance RR, Prock A, Silbey R. Comments on Classical Theory of Energy-Transfer. *Journal of Chemical Physics* 1975; **62**(6):2245-2253.

35. Chance RR, Prock A, Silbey R. Lifetime of An Emitting Molecule Near A Partially Reflecting Surface. *Journal of Chemical Physics* 1974; **60**(7):2744-2748.

36. Lakowicz JR. Radiative decay engineering 5: metal-enhanced fluorescence and plasmon emission. *Analytical Biochemistry* 2005; **337**(2):171-194.

37. Enderlein J. A theoretical investigation of single-molecule fluorescence detection on thin metallic layers. *Biophysical Journal* 2000; **78**(4):2151-2158.

38. Enderlein J. Theoretical investigation of aspects of single-molecule fluorescence detection in microcapillaries. *Cytometry* 1999; **36**(3):195-199.

39. Kuznetsova S, Zauner G, Schmauder R, Mayboroda OA, Deelder AM, Aartsma TJ, Canters GW. A Forster-resonance-energy transfer-based method for fluorescence detection of the protein redox state. *Analytical Biochemistry* 2006; **350**(1):52-60.

40. Schmauder R, Alagaratnam S, Chan C, Schmidt T, Canters GW, Aartsma TJ. Sensitive detection of the redox state of copper proteins using fluorescence. *Journal of Biological Inorganic Chemistry* 2005; **10**(6):683-687.

41. Schmauder R, Librizzi F, Canters GW, Schmidt T, Aartsma TJ. The oxidation state of a protein observed molecule-by-molecule. *Chemphyschem* 2005; **6**(7):1381-1386.

42. Davis JJ, Burgess H, Zauner G, Kuznetsova S, Salverda J, Aartsma T, Canters GW. Monitoring interfacial bioelectrochemistry using a FRET switch. *Journal of Physical Chemistry B* 2006; **110**(41):20649-20654.

43. Kuznetsova S, Zauner G, Aartsma TJ, Engelkamp H, Hatzakis N, Rowan AE, Nolte RJM, Christianen PCM, Canters GW. The enzyme mechanism of nitrite reductase studied at single-molecule level. *Proceedings of the National Academy of Sciences of the United States of America* 2008; **105**(9):3250-3255.

44. Salverda JM, Patil AV, Mizzon G, Kuznetsova S, Zauner G, Akkilic N, Canters GW, Davis JJ, Heering HA, Aartsma TJ. Fluorescent Cyclic Voltammetry of Immobilized Azurin: Direct Observation of Thermodynamic and Kinetic Heterogeneity. *Angewandte Chemie-International Edition* 2010; **49**(33):5776-5779.

45. Strianese M, Zauner G, Tepper AWJW, Bubacco L, Breukink E, Aartsma TJ, Canters GW, Tabares LC. A protein-based oxygen biosensor for high-throughput monitoring of cell growth and cell viability. *Analytical Biochemistry* 2009; **385**(2):242-248.

46. Zauner G, Strianese M, Bubacco L, Aartsma TJ, Tepper AWJW, Canters GW. Type-3 copper proteins as biocompatible and reusable oxygen sensors. *Inorganica Chimica Acta* 2008; **361**(4):1116-1121.

47. Zauner G, Lonardi E, Bubacco L, Aartsma TJ, Canters GW, Tepper AWJW. Tryptophan-to-dye fluorescence energy transfer applied to oxygen sensing by using type-3 copper proteins. *Chemistry-A European Journal* 2007; **13**(25):7085-7090.

48. Vandekamp M, Hali FC, Rosato N, Agro AF, Canters GW. Purification and Characterization of A Nonreconstitutable Azurin, Obtained by Heterologous Expression of the Pseudomonas-Aeruginosa Azu Gene in Escherichia-Coli. *Biochimica et Biophysica Acta* 1990; **1019**(3):283-292.

49. Freeman RG, Grabar KC, Allison KJ, Bright RM, Davis JA, Guthrie AP, Hommer MB, Jackson MA, Smith PC, Walter DG, Natan MJ. Self-Assembled Metal Colloid Monolayers - An Approach to Sers Substrates. *Science* 1995; **267**(5204):1629-1632.

50. Daniel MC, Astruc D. Gold nanoparticles: Assembly, supramolecular chemistry, quantum-size-related properties, and applications toward biology, catalysis, and nanotechnology. *Chemical Reviews* 2004; **104**(1):293-346.

51. Delfino I, Cannistraro S. Optical investigation of the electron transfer protein azurin-gold nanoparticle system. *Biophysical Chemistry* 2009; **139**(1):1-7.

52. Benda A, Hof M, Wahl M, Patting M, Erdmann R, Kapusta P. TCSPC upgrade of a confocal FCS microscope. *Review of Scientific Instruments* 2005; **76**(3).

53. Gaiduk A, Ruijgrok PV, Yorulmaz M, Orrit M. Detection limits in photothermal microscopy. *Chemical Science* 2010; **1**(3):343-350.

54. Jain PK, Lee KS, El-Sayed IH, El-Sayed MA. Calculated absorption and scattering properties of gold nanoparticles of different size, shape, and composition: Applications in biological imaging and biomedicine. *Journal of Physical Chemistry B* 2006; **110**(14):7238-7248.

55. Kolczak, U., Dennison, C, Messerschmidt, A., and Canters, G. W. Azurin and azurin mutants. Messerschmidt, A., Huber, R., Poulos, T., and Wieghardt, K. 1170-1194. 2001. John Wiley & Sons. Handbook of Metalloproteins.

56. Pompa PP, Chiuri R, Manna L, Pellegrino T, del Mercato LL, Parak WJ, Calabi F, Cingolani R, Rinaldi R. Fluorescence resonance energy transfer induced by conjugation of metalloproteins to nanoparticles. *Chemical Physics Letters* 2006; **417**(4-6):351-357.

57. Pastoriza-Santos I, Gomez D, Perez-Juste J, Liz-Marzan LM, Mulvaney P. Optical properties of metal nanoparticle coated silica spheres: a simple effective medium approach. *Physical Chemistry Chemical Physics* 2004; **6**(21):5056-5060.

58. Lunt EAM, Pitter MC, O'Shea P. Quantitative Studies of the Interactions of Metalloproteins with Gold Nanoparticles: Identification of Dominant Properties of the Protein that Underlies the Spectral Changes. *Langmuir* 2009; **25**(17):10100-10106.

59. Nar H, Messerschmidt A, Huber R, Vandekamp M, Canters GW. Crystal-Structure Analysis of Oxidized Pseudomonas-Aeruginosa Azurin at Ph 5.5 and Ph 9.0 - A Ph-Induced Conformational Transition Involves A Peptide-Bond Flip. *Journal of Molecular Biology* 1991; **221**(3):765-772.

60. Sapsford KE, Berti L, Medintz IL. Materials for fluorescence resonance energy transfer analysis: Beyond traditional donor-acceptor combinations. *Angewandte Chemie-International Edition* 2006; **45**(28):4562-4588.

61. Elmalk AT, Salverda JM, Tabares LC, Canters GW, Aartsma TJ. Probing redox proteins on a gold surface by single molecule fluorescence spectroscopy. *Journal of Chemical Physics* 2012; **136**:235101.

62. Zhang J, Lakowicz JR. Metal-enhanced fluorescence of an organic fluorophore using gold particles. *Optics Express* 2007; **15**(5):2598-2606.

63. Chowdhury MH, Ray K, Aslan K, Lakowicz JR, Geddes CD. Metal-enhanced fluorescence of phycobiliproteins from heterogeneous plasmonic nanostructures. *Journal of Physical Chemistry C* 2007; **111**(51):18856-18863.

64. Aslan K, Malyn SN, Geddes CD. Angular-dependent metal-enhanced fluorescence from silver island films. *Chemical Physics Letters* 2008; **453**(4-6):222-228.

65. Fu Y, Lakowicz JR. Single-molecule studies of enhanced fluorescence on silver island films. *Plasmonics* 2007; **2**(1):1-4.

66. Kinkhabwala A, Yu ZF, Fan SH, Avlasevich Y, Mullen K, Moerner WE. Large single-molecule fluorescence enhancements produced by a bowtie nanoantenna. *Nature Photonics* 2009; **3**(11):654-657.

67. Le Moal E, Leveque-Fort S, Potier MC, Fort E. Nanoroughened plasmonic films for enhanced biosensing detection. *Nanotechnology* 2009; **20**(22).

68. Mie G. *Annals of Physics* 1908; **25**:377.

69. Aroca R, Kovacs GJ, Jennings CA, Loutfy RO, Vincett PS. Fluorescence Enhancement from Langmuir-Blodgett Monolayers on Silver Island Films. *Langmuir* 1988; **4**(3):518-521.

70. Biteen JS, Pacifici D, Lewis NS, Atwater HA. Enhanced radiative emission rate and quantum efficiency in coupled silicon nanocrystal-nanostructured gold emitters. *Nano Letters* 2005; **5**(9):1768-1773.

71. Chumanov G, Sokolov K, Gregory BW, Cotton TM. Colloidal Metal-Films As A Substrate for Surface-Enhanced Spectroscopy. *Journal of Physical Chemistry* 1995; **99**(23):9466-9471.

72. Wokaun A, Lutz HP, King AP, Wild UP, Ernst RR. Energy-Transfer in Surface Enhanced Luminescence. *Journal of Chemical Physics* 1983; **79**(1):509-514.

73. Shen H, Lu GW, Ou MG, Marquette CA, Ledoux G, Roux S, Tillement O, Perriat P, Cheng BL, Chen ZH. How the morphology of biochips roughness increases surface-enhanced chemiluminescence. *Chemical Physics Letters* 2007; **439**(1-3):105-109.

74. Estrada LC, Roberti MJ, Simoncelli S, Levi V, Aramendia PF, Martinez OE. Detection of Low Quantum Yield Fluorophores and Improved Imaging Times Using Metallic Nanoparticles. *Journal of Physical Chemistry B* 2012; **116**(7):2306-2313.

75. Zijlstra P, Paulo PMR, Yu K, Xu Q-H, Orrit M. Chemical Interface Damping in Single Nanorods and Its Near Elimination by Tip-Specific Functionalization. *Angewandte Chemie-International Edition* 2012; **51**:8352-8355.

76. Kelly KL, Coronado E, Zhao LL, Schatz GC. The optical properties of metal nanoparticles: The influence of size, shape, and dielectric environment. *Journal of Physical Chemistry B* 2003; **107**(3):668-677.